Journal of Photochemistry & Photobiology, B: Biology 226 (2022) 112354

Contents lists available at ScienceDirect

Journal of Photochemistry & Photobiology, B: Biology

journal homepage: www.elsevier.com/locate/jphotobiol

Fabrication of Cu_2MoS_4 decorated WO_3 nano heterojunction embedded on chitosan: Robust photocatalytic efficiency, antibacterial performance, and bacteria detection by peroxidase activity

Haitao Lin [a], Tao Li [a,*], Baadal Jushi Janani [b,*], Ali Fakhri [c]

[a] Yuxi Normal University, Yuxi, Yunnan 653100, China
[b] Department of Chemistry, Academy of Materials Science, Navi Mumbai, India
[c] Nanotechnology Laboratory, Nano Smart Science Institute, Tehran, Iran

A R T I C L E I N F O

Keywords:
Cu_2MoS_4/WO_3/Chitosan
Photocatalysis
Antibacterial
Colorimetric

A B S T R A C T

In this study, the Cu_2MoS_4/WO_3 supported on chitosan was prepared by precipitation method, and applied to photocatalyst, antibacterial agent and biosensor. The presence of WO_3 and Cu_2MoS_4 crystals were confirmed by XRD analysis. The elemental information was investigated by EDS. FTIR spectra shows the presence of chitosan in nanocomposites. The as-synthesized Cu_2MoS_4/WO_3/Chitosan nanocomposites has a bandgap of 2.18 eV and it is effective for visible light condition. The average particle size of the Cu_2MoS_4/WO_3/Chitosan is 71 nm. The photocatalysis activity Cu_2MoS_4/WO_3/Chitosan was higher than Cu_2MoS_4 or WO_3.The Cu_2MoS_4/WO_3/Chitosan nanocomposites shows the highest efficiency (100%) in photocatalysis degradation of dye under visible light irradiation in 80 min. The $\bullet O^{2-}$ plays a main role in degradation process. The as-synthesized Cu_2MoS_4/WO_3/Chitosan nanocomposites depicted the antibacterial activity toward G+/− bacteria. Determination of *enterococcus faecalis* is important for human health. The DNA template was used to the Cu_2MoS_4/WO_3/Chitosan nanocomposites and applied in detection of *enterococcus faecalis* by H_2O_2 and 3,3′,5,5′ -tetramethylbenzidine in peroxidase like activity. The detection limit of *enterococcus faecalis* by DNA-Cu_2MoS_4/WO_3/Chitosan in peroxidase-like catalysis was about 55 CFU/mL. Therefore, the Cu_2MoS_4/WO_3/Chitosan can be applied in the photocatalysis, bactericidal and peroxidase process.

1. Introduction

The semiconductor nanoparticles have been studied for different photocatalysis efficiency such organic pollution degradation, and toxic metal removal [1,2]. In the photocatalysis system, nano semiconductor absorb light and generate e^-/h^+ pairs for different redox reactions [3,4]. The e^-/h^+ pair generation improves the photocatalysis efficiency. In degradation process, the pollutants can degrade without the reagents and decreased the secondary waste production [4].

Tungsten trioxide is the potent semiconductors (band gap: 3.6 eV) [5,6]. WO_3 is stable for fabrication of photocatalysis system at room temperature [5]. However, WO_3 has a poor charge transport for photo-generated e^-/h^+ pairs, due to wide band gap. Then, the best method for modification of photocatalysis efficiency of the semiconductor oxide is combining with the nano semiconductor sulfide [7–10]. Cu_2MoS_4 is semiconductor with a narrow band gap energy [11]. The Cu_2MoS_4 is extensively applicable in the photochemical and the electronic devices [12]. They are more potent to be fabricated as heterostructures owing to the generation of photoinduced charge carriers [12]. The Cu_2MoS_4 is excellent photocatalyst for contributes in the hybrid photocatalyst and used in the degradation and decomposition of the dyestuffs [11].

Previous studies have shown the activity of photocatalyst supported on carbon structures [13,14]. Chitosan was applied as a supporter for the nano semiconductor sulfide and oxides due to the substantial properties like biodegradability and stability. Carbon substrate presents more active sites for the photocatalysis reaction [13]. The various photocatalysts nanohybrid was studied including $Ag_2S/NiTiO_3$/Chitosan [7], Ag_3PO_4-$FeTiO_3$/glycol chitosan [8], CuS/PVA-chitosan [15], Cr_2S_3/Co_3O_4/PEG-chitosan [16], CoS_2-CeO_2/cellulose-chitosan [17], and MnS_2/chitosan [18].

Catalytically nanomaterials have studied as a main tool for detection of biological and bacterial, due to high stability, and excellent catalytic

* Corresponding authors.
E-mail addresses: vvxc60@163.com (T. Li), bajujanani@gmail.com (B.J. Janani).

https://doi.org/10.1016/j.jphotobiol.2021.112354
Received 26 July 2021; Received in revised form 25 October 2021; Accepted 3 November 2021
Available online 7 November 2021

performance [19]. The various type of nanomaterials such as carbon substrate [20], metal oxides/sulfide [21], and metal nanoparticles [22] were showing peroxidase activities. However, ultra-sensitive and cost-effective colorimetric biosensors are need for detection of bacteria such as *enterococcus faecalis* with pathogenic properties for human health. DNA is a template for nanomaterials in biosensors [23]. Nanoparticles and DNA template with peroxidase activity have applied for the biological detection due to cost-efficient, and facile devices [23]. Colorimetric via biosensor is the best analysis for determination of biomolecules due to visible color change response.

This study provides the new synthesis method of $Cu_2MoS_4/WO_3/$Chitosan. The nanohybrid was characterized by various analysis. The photocatalysis efficiency was improved by the nanohybrid supported on carbon frame compared to pure Cu_2MoS_4 and WO_3. The photocatalytic performance was evaluated with crystal violet degradation under visible light. The bactericidal properties of the $Cu_2MoS_4/WO_3/$Chitosan was tested toward G+/− bacteria. The DNA template-$Cu_2MoS_4/WO_3/$Chitosan biosensor was applied for detection of *enterococcus faecalis* bacteria by using colorimetric peroxidase method. The real samples were studied for sensitivity/selectivity evaluation in bacterial detection.

2. Experimental

2.1. Materials

The materials and reagents with highly analytical grade were obtained from Merck (Germany).

2.2. Synthesis of WO_3 and $Cu_2MoS_4/WO_3/$Chitosan

WO_3 was synthesized by precipitation method from ammonium tungstate hydrate (0.1 M) was mixed as precursor in 10%*v*/v, HNO_3. The above solution is homogenized under heat for 40 min, and then 0.2 M of NH_4OH solution was added drop by drop. Then, the solution was transferred to reflux system and heated at 130 °C for 5 h to obtain WO_3.

The $Cu_2MoS_4/WO_3/$Chitosan was synthesized by using ultrasonic method. $[NH_4]_2MoS_4$ was prepared by bubbling H_2S through a suspension of $[NH_4]_6[Mo_7O_{24}].4H_2O$ in ammonia aqueous solution. Then, WO_3 particles was dispersed in distilled water and sonicated for 60 min, and the $(NH_4)_2MoS_4$ and CuCl solution (0.1 M) and chitosan (2%) were added. Then, the mixture was sonicated for 30 min. In the stirring, the CTAB (0.4 M) was added drop by drop to the mixture. After that, the mixture was transferred to reflux device and heated at 120 °C for 5 h. Precipitate was separated and washed with deionized water/ethanol. The product was dried at 130 °C for 50 min.

2.3. Characterization Instrumental

Crystal structural analysis of the prepared material was identified by XRD analysis (PANalytical diffractometer). The morphology data of the prepared material was studied by FESEM technique (MIRA 3 TESCAN). In order to identify the chemical elemental of the prepared material, EDS analysis was conducted. Quantachrome instruments was applied for determine surface area information. The optical properties of the prepared material was studied by UV–vis spectrophotometry (Agilent Cary 60). The functional agents in the prepared material was investigated by Fourier transform infrared spectroscopy (Thermo Nicolet 380).

2.4. Photocatalysis Setup

The photocatalytic activity of $Cu_2MoS_4/WO_3/$Chitosan was tested by using degradation of crystal violet (CV) dye under visible lamps (halogen lamp, 500 W) irradiation. The $Cu_2MoS_4/WO_3/$Chitosan (1 g/L) were dispersed in aqueous CV solution (15 mg/L). The dark condition was used to attain equilibrium reaction. The samples were collected every 5 min and spectrophotometrically (λ_{max} = 590 nm) tested to find the residual dye concentration after photocatalysis reaction. The 1 mL of different scavengers such as $AgNO_3$, EDTA, *p*-benzoquinone, and Isopropyl alcohol (1 mM) were applied for trapping the e^-, h^+, $\bullet O^{2-}$, and $\bullet$OH, respectively, in photocatalysis system. The catalyst reusability was studied in four photocatalytic cycles in CV degradation reaction by the $Cu_2MoS_4/WO_3/$Chitosan.

2.5. Antibacterial Test

The as-synthesized $Cu_2MoS_4/WO_3/$Chitosan was applied toward *Streptococcus pneumoniae* and *Pseudomonas aeruginosa* to evaluation of bactericidal properties. The bacterial were incubated in LB broth for 10 h and separated by the centrifugation. The different dosage of $Cu_2MoS_4/WO_3/$Chitosan (1, 2, 4, 8, and 20 mg/L) were used in this test. Then, the bacteria was interacted with $Cu_2MoS_4/WO_3/$Chitosan for 4 h, and the viable cells left was determined by plate count methods. The reduction in bacterial cell number was distinguished. The experiment was carried out in triplicate [24–30].

2.6. Colorimetric Peroxidase Test

In the first stage, $Cu_2MoS_4/WO_3/$Chitosan was dispersed in phosphate buffer (PSB) solution (pH 7.0), and the mixture was augmented to the template DNA solution (10 μL, 2 μM). The suspension was vigorously stirred at 38 °C for 5 h. The reactor was prepared through the 15 μL of H_2O_2 (3 mM), 15 μL of TMB (3 mM) and DNA-$Cu_2MoS_4/WO_3/$Chitosan for 30 min and incubated at 38 °C. For bacterial detection, various concentrations of *enterococcus faecalis* were added to the DNA-$Cu_2MoS_4/WO_3/$Chitosan and incubated at 28 °C for 30 min. After that, the supernatant was separated from the solution and TMB + H_2O_2 were applied in colorimetric peroxidase test. The bacteria colonies were diluted in PSB and the absorbance was monitored with UV–Vis spectroscopy technique. The human serum, milk and fruit juice samples were applied for detection of bacteria from real samples. Known concentration (10^6 CFU/mL) was spiked to the real samples. The selectivity test for bacterial detection was conducted in the presence of the different bacteria strains.

3. Results and Discussion

3.1. Characterization of $Cu_2MoS_4/WO_3/$Chitosan

FESEM image depicts an obvious structure, agglomerated particle of $Cu_2MoS_4/WO_3/$Chitosan (Fig. 1A). The image displays the formation of the particle of Cu_2MoS_4 on WO_3 surface. As can be seen that there are interface between WO_3 and Cu_2MoS_4 and supported on chitosan, due to electron transfer between materials, and the well-defined structure in $Cu_2MoS_4/WO_3/$Chitosan was formed. Additional, the EDS analysis was studied for checking the elementals information in composites. Fig. 1B depicts that the EDS spectra of the $Cu_2MoS_4/WO_3/$Chitosan, and confirmed the presence of tungsten, oxygen, molybdenum, sulfur, cupper, and carbon with weight percent about 22.51, 16.21, 15.98, 13.25, 14.74, and 16.32%, respectively. The average particle size of the $Cu_2MoS_4/WO_3/$Chitosan was shown in Fig. 1C, and is 71 nm. BET technique was conducted to measure the active surface area of the prepared WO_3, Cu_2MoS_4, and $Cu_2MoS_4/WO_3/$Chitosan. The active surface area of WO_3, Cu_2MoS_4, and $Cu_2MoS_4/WO_3/$Chitosan were determined as 43.25, 61.87 and 140.36 m^2/g, respectively. The presence of chitosan in $Cu_2MoS_4/WO_3/$Chitosan can be increase active site in composites, and leads improvement in photocatalysis system.

XRD technique was applied to identify the crystal phase of $Cu_2MoS_4/WO_3/$Chitosan and the XRD patterns of WO_3, Cu_2MoS_4 and $Cu_2MoS_4/WO_3/$Chitosan are displayed in Fig. 2. The XRD pattern of WO_3 shown peaks at 2θ value of 19.5°,22.88°, 23.15°, 24.5°, 27.0°, 27.6°,33.8°, 43.5°, 49.7°, 51,80°. The XRD patterns fitted well with standard card PDF 83–0950 [6]. The peaks observed at 2θ angle of s 17.31, 19.00,

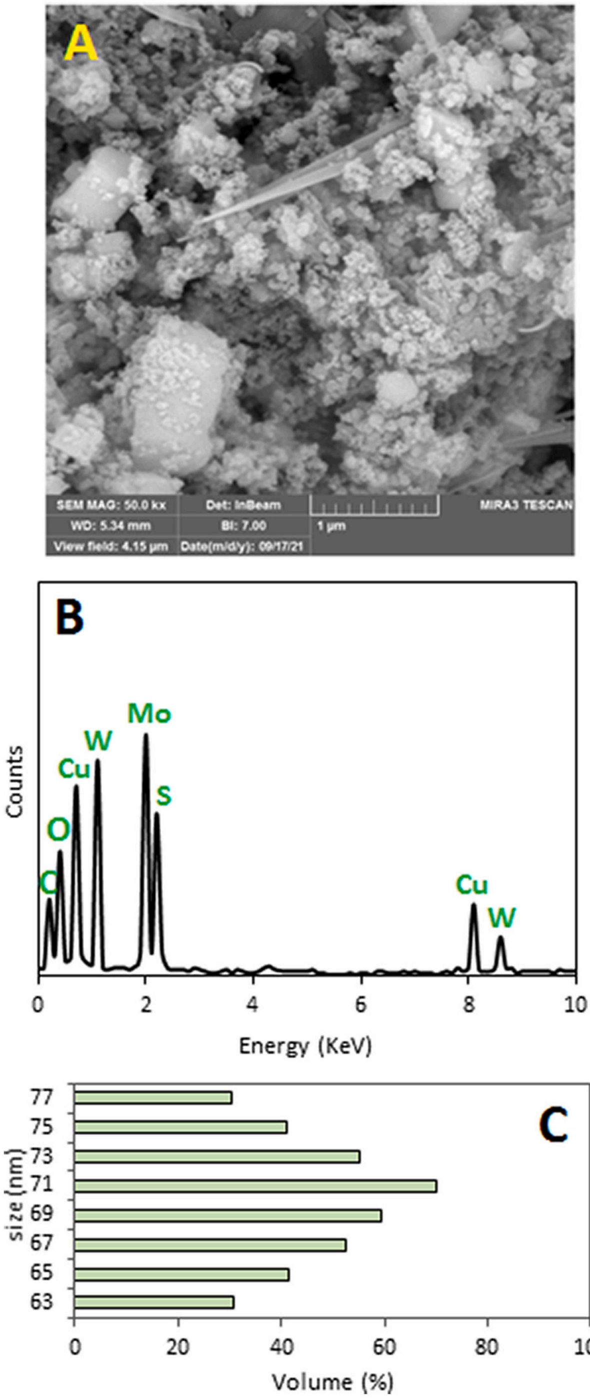

Fig. 1. FESEM image (A), and EDS spectra of Cu_2MoS_4/WO_3/Chitosan nanocomposites.

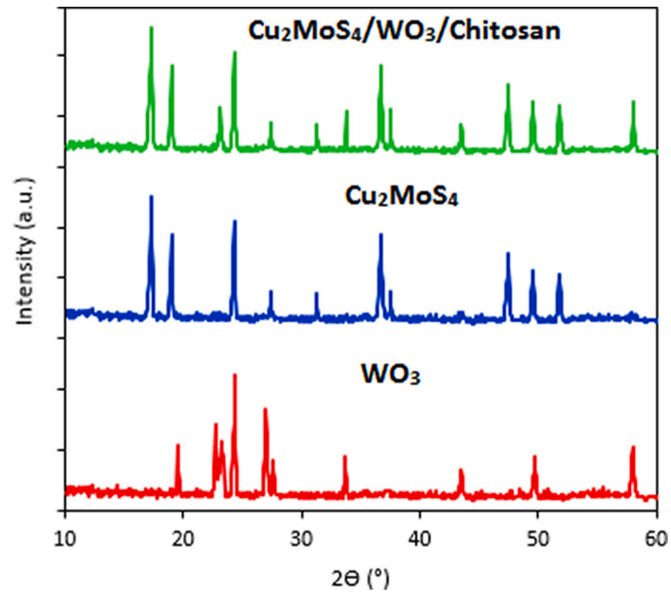

Fig. 2. XRD pattern of WO_3, Cu_2MoS_4 and Cu_2MoS_4/WO_3/Chitosan nanocomposites.

24.32, 27.42, 31.13, 36.71, 37.35, 47.52, 49.60, 53.05, and 57.21° denotes Cu_2MoS_4 presence. The obtained peaks fitted well with standard card PDF 81–1159 [12]. The XRD pattern of Cu_2MoS_4/WO_3/Chitosan have high intensity peaks of both Cu_2MoS_4 and WO_3.

Fourier transform infrared spectroscopy (FTIR) analysis was conducted to study the vibrational transition for various bonds in the prepared materials (Fig. 3A). In Cu_2MoS_4/WO_3/Chitosan, the vibration of O—H bond was detected by the wide peak at 3579 cm^{-1} due to moisture absorption. The stretching metal sulfide or oxide bonds was observed at 526 to 629 cm^{-1} [13]. The amine vibration and hydroxyl vibration of the chitosan were observed at 3405 cm^{-1} [15]. The peak of oxygen stretch from chitosan was apperceived at 1088 cm^{-1} [15].

Kubelka-Munk plot was applied to distinguish the optical behaviors of the as-synthesized nanomaterials and depicted in Fig. 3B. Kubelka-Munk plot was studied by using the UV–vis analysis. As a photon energy function, the Kubelka-Munk plot shows the band gap values [31]. The as-synthesized Cu_2MoS_4/WO_3/Chitosan nanocomposites was active in visible light region, and shows that the band gap was 2.18 eV, moreover, the band gap of WO_3 and Cu_2MoS_4 were 3.27 and 2.60 eV, respectively. From the results, the as-synthesized Cu_2MoS_4/WO_3/Chitosan nanocomposites can be highly active in visible light absorption for photocatalytic process [32,33].

Fig. 3C denotes the photocurrent properties of WO_3, Cu_2MoS_4 and Cu_2MoS_4/WO_3/Chitosan under light illumination. Specifically, the photocurrent response of the Cu_2MoS_4/WO_3/Chitosan is better than the WO_3, and Cu_2MoS_4, illustrating the superb light activation of the Cu_2MoS_4/WO_3/Chitosan. The photocurrent response depicts that the presence of Cu_2MoS_4 nanostructure and chitosan improved the charge transportation and reduces the recombination rate of e^-/h^+. Therefore, the prepared Cu_2MoS_4/WO_3/Chitosan can be presents the high activity under light irradiation system such as photocatalysis reaction.

3.2. Photocatalysis Process

The photocatalytic response of as-synthesized of the WO_3, Cu_2MoS_4 and Cu_2MoS_4/WO_3/Chitosan were investigated using CV dye degradation under visible light irradiation. Fig. 4A shows the photocatalysis properties of the prepared catalyst in different reaction time. As can be seen observed that the dark condition shows the removal amount range 8–25% for three catalysts. The removal amount of Cu_2MoS_4/WO_3/Chitosan was higher than the WO_3, and Cu_2MoS_4, due to the presence of high active surface area in Cu_2MoS_4/WO_3/Chitosan. From Fig. 4A, the photocatalysis efficiency of Cu_2MoS_4/WO_3/Chitosan was 100% for degradation of CV under visible light in 80 min as reaction time. The photocatalysis amount of Cu_2MoS_4/WO_3/Chitosan was higher than the WO_3 (61.34%) and Cu_2MoS_4 (80.13%) due to the lowest band gap of Cu_2MoS_4/WO_3/Chitosan, in compared to other catalysts. The enhanced photocatalysis performance shows that the high activity of Cu_2MoS_4/WO_3/Chitosan in visible light range due to the reduced e^-/h^+ recombination [33,34].

Photo-degradation of CV was done using the prepared Cu_2MoS_4/WO_3/Chitosan catalyst from each cycle. Degradation amount of each

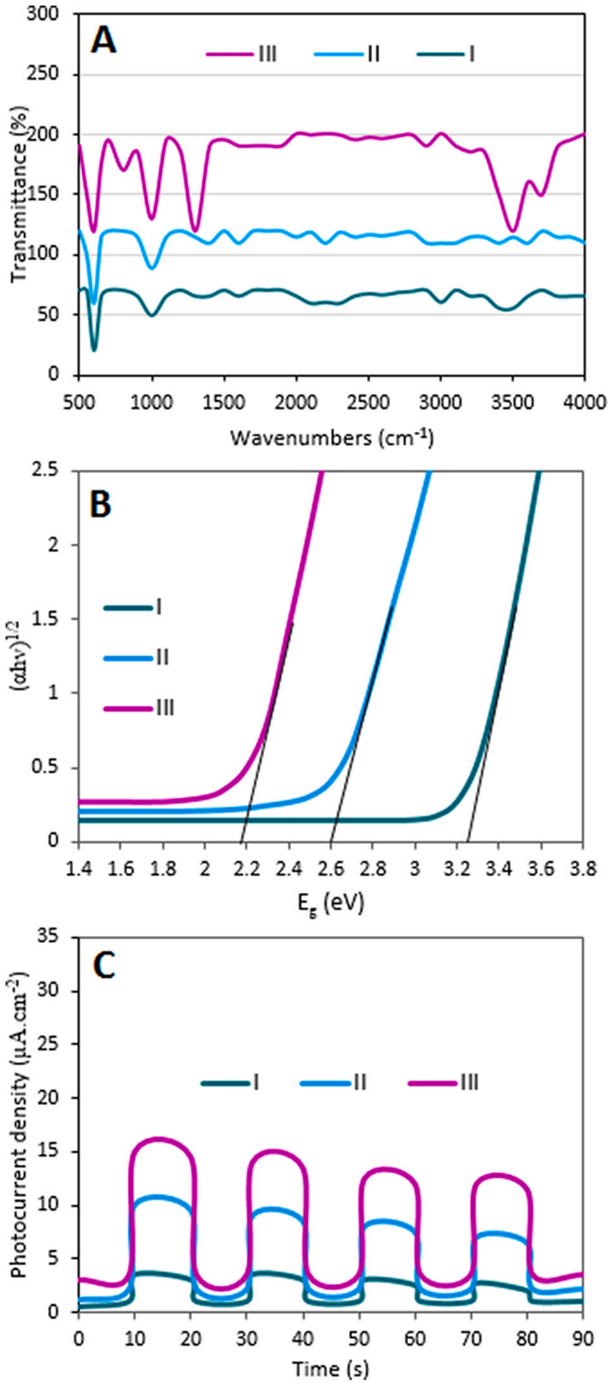

Fig. 3. FTIR spectrum (A), Kubelka-Munk plot (B), and Transient photocurrent responses (C) of the prepared materials.

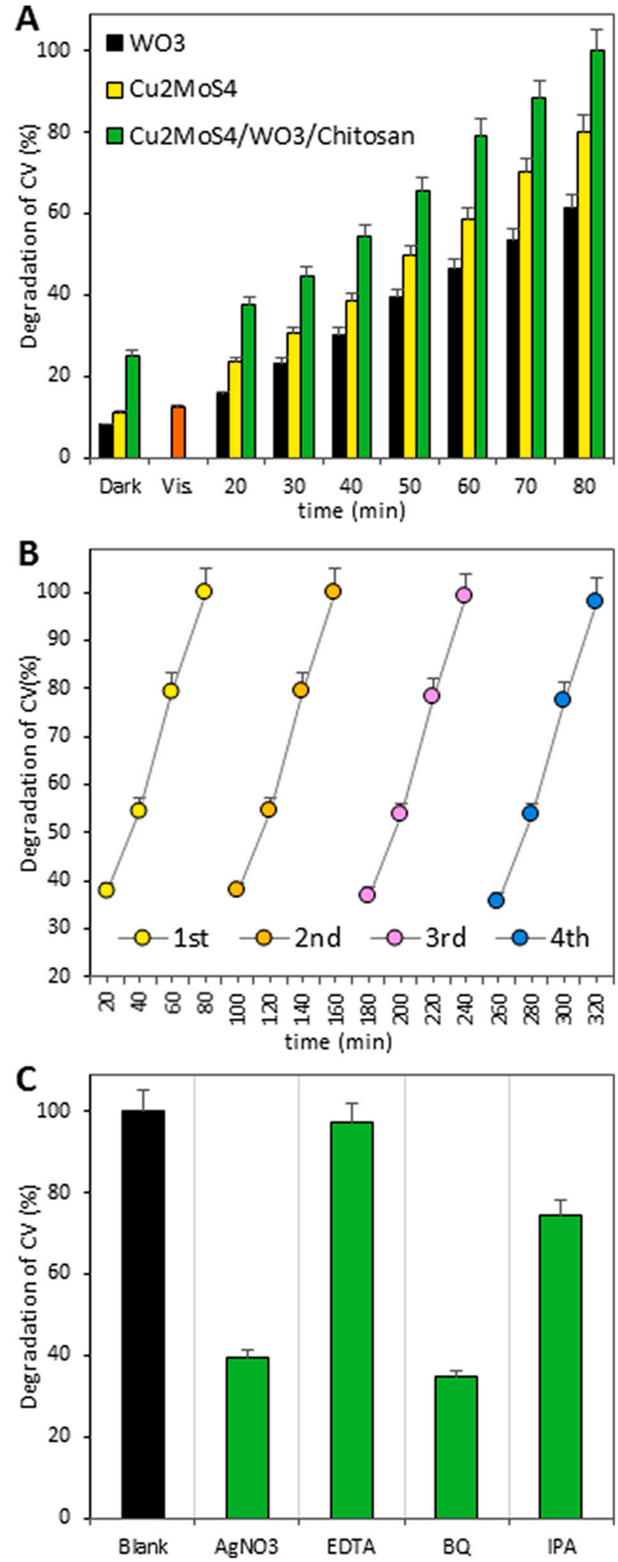

Fig. 4. Photocatalysis activity in different times (A), Stability analysis (B), and Scavenging analysis (C) for degradation of CV by the prepared materials under visible light irradiation.

cycle was determined. Fig. 4B shows the photodegradation efficiency in sixth cycles. The degradation amount of first cycle was 100.0% and for 4th cycle it was 98.0%. The decrease in decomposition performance was negligible. The results depicted that Cu_2MoS_4/WO_3/Chitosan has superb photo-stability and reusability. Scavengers are utilized for capturing active species and decrease in photocatalysis performance [35–52]. Here $AgNO_3$, EDTA, BQ, and IPA were used for quenching the e^-, h^+, $\bullet O^{2-}$, and $\bullet$OH, respectively. Fig. 4C illustrates the effect of scavengers in degradation of CV and it was found that degradation reduces in presence of BQ. Therefore, the $\cdot O_2^-$ plays the main role in degradation of CV by Cu_2MoS_4/WO_3/Chitosan. In the reaction, the e^-/h^+ pairs generates from light irradiation. The e^- reacts with oxygen to $\cdot O_2^-$ free radical. Under visible light irradiation, e^- can transfer from the catholic CB of WO_3 to the more anionic CB of Cu_2MoS_4. The charge carriers are separated and increases the performance of the interfacial charge transfer. The Chitosan provides more active sites and enhance charge separation [53,54].

3.3. Antibacterial Properties

Antibacterial activity of the as-synthesized particles was tested against *Streptococcus pneumoniae* and *Pseudomonas aeruginosa* and it is depicted in Fig. 5. At 20 mg/L, Cu_2MoS_4/WO_3/Chitosan shows 100% toxicity against two bacterial. When nanomaterials concentration was reduced, the toxicity too decreased. The toxicity against *P. aeruginosa* was higher than when compared to *S. pneumoniae*. This is due to the thin cell wall of G^- bacteria and that allows high Cu_2MoS_4/WO_3/Chitosan penetration. Similar reports on the bactericidal influence of metal oxide/sulfide for cell damage by electrostatic interaction [55,56].

3.4. Colorimetric Peroxidase Activity for Detection of E. faecalis

Fig. 6A depicts that the peroxidase activity of DNA-Cu_2MoS_4/WO_3/Chitosan, *E. faecalis*, and DNA-Cu_2MoS_4/WO_3/Chitosan + *E. faecalis* were evaluated in the presence of TMB & H_2O_2. As can be seen that the absorbance of DNA-Cu_2MoS_4/WO_3/Chitosan was higher than DNA-Cu_2MoS_4/WO_3/Chitosan + *E. faecalis* and *E. faecalis*. The UV–vis spectra of *E. faecalis* shows no peak absorbance, due to TMB was not oxidized with H_2O_2. The result denotes that the prepared DNA-Cu_2MoS_4/WO_3/Chitosan can be utilized for colorimetric detection of *E. faecalis*. Fig. 6B depicts that the absorbance was decreased, while that the *E. faecalis*

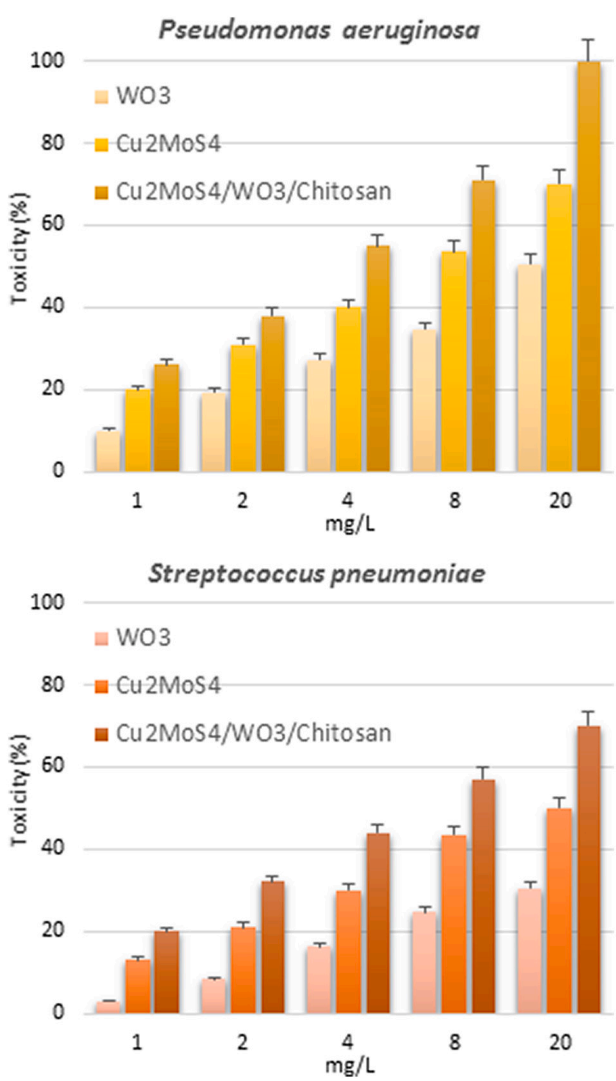

Fig. 5. The antibacterial effect of the prepared materials toward *Streptococcus pneumoniae* (A) and *Pseudomonas aeruginosa* (B).

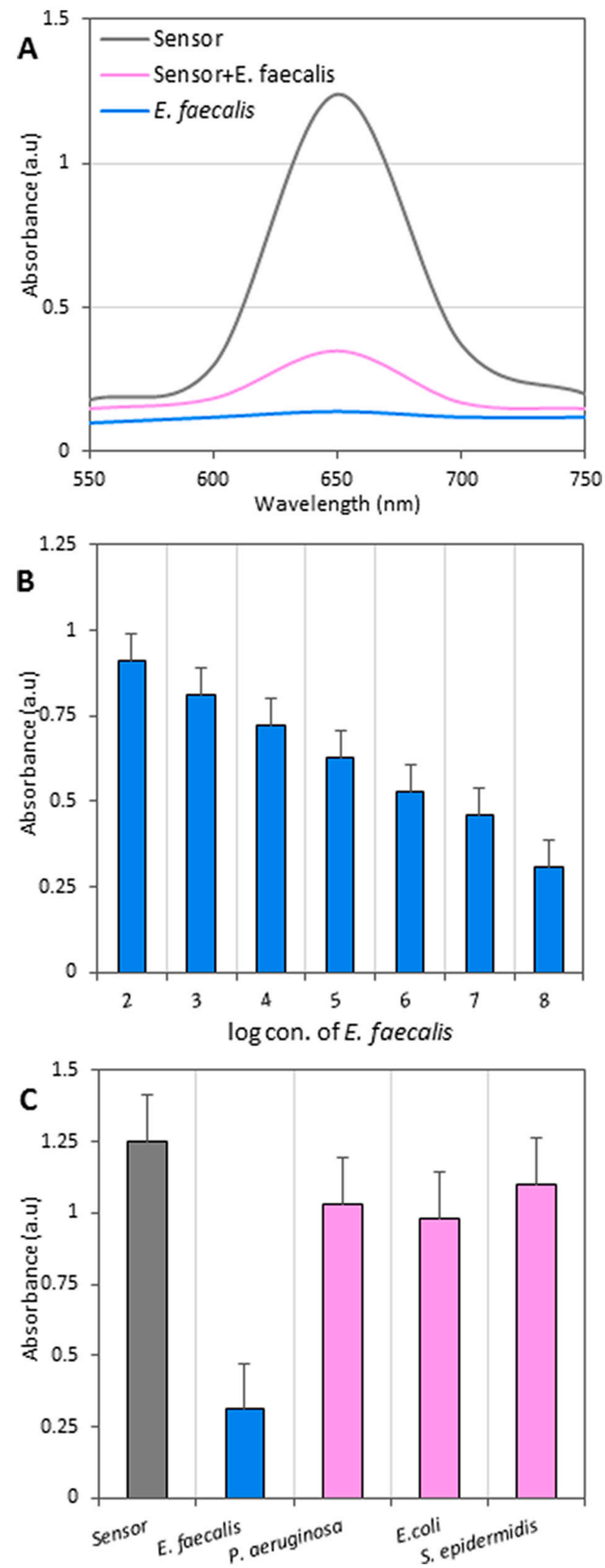

Fig. 6. The UV–vis absorption spectra of peroxidase activity (A), the absorbance values for interaction of DNA-Cu_2MoS_4/WO_3/Chitosan with different *E. faecalis* concentrations in peroxidase process, and (C), the selectivity *E. faecalis* detection in the presence of different bacteria (C) by DNA-Cu_2MoS_4/WO_3/Chitosan.

concentration was increased from 10^2 to 10^8 CFU/mL. The limit of detection (LOD) was determined from the calibration curve for the *E. faecalis* concentration [$Y = -0.1502 X + 0.982$, $R^2 = 0.9971$] [56]. The LOD was calculated as 55 CFU/mL. The colorimetric detection of *E. faecalis* by DNA-Cu_2MoS_4/WO_3/Chitosan was studied in the presence of different bacteria such as *E.coli*, *P. aeruginosa*, and *S. epidermidis*. Fig. 6C displays that the absorbance intensity for *E. faecalis* was lower than other bacteria, which that shows the ultra-selectivity properties of the DNA-Cu_2MoS_4/WO_3/Chitosan for detection of *E. faecalis* [56]. The colorimetric detection of *E. faecalis* by DNA-Cu_2MoS_4/WO_3/Chitosan was studied from real sample. The test was carried out by the human serum, and lemon juice as real samples. The spiked concentration of *E. faecalis* was 10^5 CFU/mL for selected real samples. The responses of test showed that the obtained concentration of *E. faecalis* were 0.90×10^5 CFU/mL and 0.99×10^5 CFU/mL for the human serum, and lemon juice samples, respectively, after detection process. This analysis shows excellent response for detection of bacteria from real samples with the recovery rate about 90.0–99.0%.

4. Conclusions

The Cu_2MoS_4/WO_3/Chitosan has been synthesized by chemically method and improved the photocatalytic activity compared to the WO_3 and Cu_2MoS_4 particles. The as-prepared nanomaterials was characterized by different techniques. Degradation of crystal violet dye was conducted by the prepared nanomaterials under visible light. The WO_3 and Cu_2MoS_4 particles exhibited lesser response, while when the Cu_2MoS_4/WO_3/Chitosan shows the highest degradation of CV. Generated superoxide radical plays the main role in CV degradation. The photocatalyst offers greater stability and reusability even after forth cycles. Moreover, the Cu_2MoS_4/WO_3/Chitosan present excellent bactericidal activity. The results denotes that the superb peroxidase properties of DNA template- Cu_2MoS_4/WO_3/Chitosan for colorimetric detection of *E. faecalis* bacteria. The experimental responses showed that the ultra-sensitive/selective method for detection of *E. faecalis* bacteria from real samples by using of the DNA template-Cu_2MoS_4/WO_3/Chitosan in peroxidase process.

Declaration of Competing Interest

The authors declare that they have no known competing financial interests or personal relationships that could have appeared to influence the work reported in this paper.

Acknowledgement

The author thanks the management of Yuxi Normal University [NSFC (32060570)] for providing the necessary facility to carry out the research work.

References

[1] Dandan Zhu, Qixing Zhou, Action and mechanism of semiconductor photocatalysis on degradation of organic pollutants in water treatment: a review, environmental nanotechnology, Monit. Manag. 12 (2019) 100255.
[2] Haiguang Zhu, Xun Yuan, Jianping Xie, Shining photocatalysis by gold-based nanomaterials, Nano Energy 88 (2021) 106306.
[3] Qiuhui Zhu, Ke Zhang, Chuanyi Wang, Polarization-enhanced photocatalytic activity in non-centrosymmetric materials based photocatalysis: a review, Chem. Eng. J. 426 (2021) 131681.
[4] Ke Zhang, Danqing Li, Chuanyi Wang, Insights into different dimensional MXenes for photocatalysis, Chem. Eng. J. 424 (2021) 130340.
[5] Sanaz Mohammadi, Maryam Sohrabi, Ali Fakhri, Preparation and characterization of zinc and copper co-doped WO3 nanoparticles: application in photocatalysis and photobiology, J. Photochem. Photobiol. B Biol. 161 (2016) 217–221.
[6] Vinod Kumar Gupta, Shilpi Agarwal, Mahsa Naji, Pt nanoparticles decorated WO_3-MWCNTs nanocomposites: preparation, characterization, and adsorption behavior, J. Mol. Liq. 229 (2017) 514–519.
[7] Jing Wang, Jiayi Sun, Vinod Kumar Gupta, Synthesis and its characterization of silver sulfide/nickel titanate/chitosan nanocomposites for photocatalysis and water splitting under visible light, and antibacterial studies, Mater. Chem. Phys. 272 (2021) 124990.
[8] Muhammad Aqeel Ashraf, Cheng Li, Ali Fakhri, Fabrication of silver phosphate-ilmenite nanocomposites supported on glycol chitosan for visible light-driven degradation, and antimicrobial activities, Int. J. Biol. Macromol. 169 (2021) 436–442.
[9] Min Huang, Ren Zhang, Vinod Kumar Gupta, Synthesis of Co_3S_4-SnO_2/polyvinylpyrrolidone-cellulose heterojunction as highly performance catalyst for photocatalytic and antimicrobial properties under ultra-violet irradiation, Int. J. Biol. Macromol. 162 (2020) 220–228.
[10] Hongxue Wang, Guangzhi Li, Ali Fakhri, Fabrication and structural of the Ag2S-MgO/graphene oxide nanocomposites with high photocatalysis and antimicrobial activities, J. Photochem. Photobiol. B Biol. 207 (2020) 111882.
[11] Jintao Ma, Feng Zhu, Gang Xu, Enhanced visible-light photocatalytic performance of co/Ni doped Cu_2MoS_4 nanosheets for Rhodamine B and erythromycin degradation, J. Alloys Compd. 863 (2021) 158612.
[12] Liyan He, Li Guo, Xiaoli Li, Cu_2MoS_4-based magnetic composites as effective adsorbent and photocatalyst for removal of organic contaminants in water, J. Taiwan Inst. Chem. Eng. 127 (2021) 312–326.
[13] Yanni Liu, Zhou Xu, Vinod Kumar Gupta, Evaluation of synergistic effect of polyglycine functionalized gold/iron doped silver iodide for colorimetric detection, photocatalysis, drug delivery and bactericidal applications, J. Photochem. Photobiol. A Chem. 422 (2022) 113522.
[14] Ye Liu, Lina Zong, Vinod Kumar Gupta, Design and structural of Sm-doped $SbFeO_3$ nanopowders and immobilized on poly(ethylene oxide) for efficient photocatalysis and hydrogen generation under visible light irradiation, Surf. Interf. 26 (2021) 101292.
[15] Guilin Wang, Ali Fakhri, Preparation of CuS/polyvinyl alcohol-chitosan nanocomposites with photocatalysis activity and antibacterial behavior against G^+/G^- bacteria, Int. J. Biol. Macromol. 155 (2020) 36–41.
[16] Hui Pan, Hongxue Xie, Ali Fakhri, Cr_2S_3-Co_3O_4 on polyethylene glycol-chitosan nanocomposites with enhanced ultraviolet light photocatalysis activity, antibacterial and antioxidant studies, Int. J. Biol. Macromol. 148 (2020) 608–614.
[17] Xiaoyu He, Jinguo Gan, Mojgan Hosseini, Preparation of ceric oxide and cobalt sulfide-ceric oxide/cellulose-chitosan nanocomposites as a novel catalyst for efficient photocatalysis and antimicrobial study, Int. J. Biol. Macromol. 143 (2020) 952–957.
[18] Mojgan Hosseini, Mohsen Sarafbidabad, Shiva Tahami, Preparation and characterization of MnS_2/chitosan-sodium alginate and calcium alginate nanocomposites for degradation of analgesic drug: photocorrosion, mechanical, antimicrobial and antioxidant properties studies, Int. J. Biol. Macromol. 118 (2018) 1494–1500.
[19] Maha Alafeef, Parikshit Moitra, Dipanjan Pan, Nano-enabled sensing approaches for pathogenic bacterial detection, Biosens. Bioelectron. 165 (2020) 112276.
[20] Xinwei Zhao, Zhenyuan Zhang, Ce Wang, Vanadium/cobalt oxides–anchored flexible carbon nanofibers with tunable magnetism as recoverable peroxidase-like catalysts, Mater. Today Chem. 22 (2021) 100568.
[21] Duygu Yıldırım, Burcu Gökçal, Ali Tuncel, A new nanozyme with peroxidase-like activity for simultaneous phosphoprotein isolation and detection based on metal oxide affinity chromatography: monodisperse-porous cerium oxide microspheres, Chem. Eng. J. 403 (2021) 126357.
[22] Tong Li, Yuheng Bao, Weijun Tong, Boosted peroxidase-like activity of metal-organic framework nanoparticles with single atom Fe sites at low substrate concentration, Anal. Chim. Acta 1152 (2021) 338299.
[23] Qidi Sun, Nora F.Y. Tam, Jian Lin Chen, A simple paper-based colorimetric analytical device for rapid detection of *Enterococcus faecalis* under the stress of chlorophenols, Talanta 225 (2021), 121966.
[24] K. Kaviyarasu, N. Geetha, K. Kanimozhi, C. Maria Magdalane, M. Maaza, In vitro cytotoxicity effect and antibacterial performance of human lung epithelial cells A549 activity of zinc oxide doped TiO_2 nanocrystals: investigation of bio-medical application by chemical method, Mater. Sci. Eng. C 74 (2017) 325–333.
[25] C. Maria Magdalane, K. Kaviyarasu, A. Raja, M.V. Arularasu, M. Maaza, Photocatalytic decomposition effect of erbium doped cerium oxide nanostructures driven by visible light irradiation: investigation of cytotoxicity, antibacterial growth inhibition using catalyst, J. Photochem. Photobiol. B Biol. 185 (2018) 275–282.
[26] A. Mobeen Amanulla, SK., Jasmine Shahina, R. Sundaram, C. Maria Magdalane, M. Maaza, Antibacterial, magnetic, optical and humidity sensor studies of β-$CoMoO_4$ - Co_3O_4 nanocomposites and its synthesis and characterization, J. Photochem. Photobiol. B Biol. 183 (2018) 233–241.
[27] F. Fang, J. Kennedy, M. Dhillon, S. Flint, Antibacterial effect of silver nanofilm modified stainless steel surface, Int. J. Modern Phys. B 29 (10n11) (2015), 1540013.
[28] K. Kaviyarasu, C. Maria Magdalane, M. Maaza, Elucidation of photocatalysis, photoluminescence and antibacterial studies of ZnO thin films by spin coating method, J. Photochem. Photobiol. B Biol. 173 (2017) 466–475.
[29] K. Kaviyarasu, K. Kanimozhi, M. Maaza, Antiproliferative effects on human lung cell lines A549 activity of cadmium selenide nanoparticles extracted from cytotoxic effects: investigation of bio-electronic application, Mater. Sci. Eng. C 76 (2017) 1012–1025.
[30] George Amal, A. Dhayal Raj, K., Kaviyarasu, influence of solvent and precursor concentration on the properties of NiV_2O_6 nanoparticles, Surf. Interf. 21 (2020) 100711.
[31] Y. Zhang, F. Zhang, Z. Yang, H. Xue, D.D. Dionysiou, Development of a newe fficient visible-light-driven photocatalyst from SnS2 and polyvinyl chloride, J. Catal. 344 (2016) 692–700.

[32] F. Zhang, Y. Zhang, G. Zhang, Z. Yang, D.D. Dionysiou, A. Zhu, Exceptional synergistic enhancement of the photocatalytic activity of SnS_2 by coupling with polyaniline and N-doped reduced graphene oxide, Appl. Catal. B 236 (2018) 53–63.

[33] Z. Jiang, K. Chen, Y. Zhang, Y. Wang, F. Wang, G. Zhang, D.D. Dionysiou, Magnetically recoverable MgFe2O4/conjugated polyvinyl chloride derivative nanocomposite with higher visible-light photocatalytic activity for treating Cr(VI)-polluted water, Sep. Purif. Technol. 236 (2020) 116272.

[34] Shunhua Xiao, Ali Fakhri, Baadal Jushi Janani, Synthesis of spinel tin ferrite decorated on bismuth ferrite nanostructures for synergetic photocatalytic, superior drug delivery, and antibacterial efficiencies, Surf. Interf. 27 (2021) 101490.

[35] Peilian Liu, Bowen Li, Jian Zheng, Qiqi Liang, Cailing Wu, Liping Huang, Peisheng Zhang, Yongmei Jia, Sheng Wang, A novel N-nitrosation-based ratiometric fluorescent probe for highly selective imaging endogenous nitric oxide in living cells and zebrafish, Sensors Actuators B Chem. 329 (2021) 129147, https://doi.org/10.1016/j.snb.2020.129147.

[36] Mengmeng Yang, Qingquan Kong, Wei Feng, Weitang Yao, Qingyuan Wang, Hierarchical porous nitrogen, oxygen, and phosphorus ternary doped hollow biomass carbon spheres for high-speed and long-life potassium storage, Carbon Energy. (2021), https://doi.org/10.1002/cey2.157.

[37] Wen-Yong Huang, Guo-Qing Wang, Wen-Hao Li, Ting-Ting Li, Guang-Jun Ji, Shi-Cheng Ren, Miao Jiang, Li Yan, Hai-Tao Tang, Ying-Ming Pan, Yun-Jie Ding, Porous ligand creates new reaction route: bifunctional single-atom palladium catalyst for selective distannylation of terminal alkynes, Chem 6 (9) (2020) 2300–2313, https://doi.org/10.1016/j.chempr.2020.06.020.

[38] Jing-Zhao Cheng, Zhi-Rong Tan, Yu-Qin Xing, Zhao-Qi Shen, Yu-Jie Zhang, Li-Lin Liu, Kai Yang, Shi-Yong Liu, Exfoliated conjugated porous polymer nanosheets for highly efficient photocatalytic hydrogen evolution, J. Mater. Chem. A 9 (2021) 5787–5795, https://doi.org/10.1039/D0TA11479K.

[39] Liu Hu, Xue-Xiang Li, Xin-Yang Liu, Zhen-Hui Ma, Zhou-Yang Yin, Wei-Wei Yang, Yong-Sheng Yu, Schiff-base-rich g-C_xN_4 supported PdAg nanowires as an efficient Mott–Schottky catalyst boosting photocatalytic dehydrogenation of formic acid, Rare Metals 40 (4) (2021) 808–816, https://doi.org/10.1007/s12598-020-01637-5.

[40] Ruo-Yan Miao, Xue-Xiang Li, Qian Lei, Liu Hu, Zhen-Hui Ma, Xu-Dong Liu, Zhou-Yang Yin, Zuo-Bin Tang, Zhang Liang, Yu-Hong Tian, Yuhong Tian, Room-temperature hydrogen spillover achieving stoichiometric hydrogenation of NO3− and NO2− into N2 over CuPd nanowire network, Rare Metals (2022), https://doi.org/10.1007/s12598-021-01854-6.

[41] Kelin Hu, Feipeng Wang, Zijia Shen, Hongcheng Liu, Jianglin Xiong, Ternary heterojunctions synthesis and sensing mechanism of Pd/ZnO–SnO_2 hollow nanofibers with enhanced H_2 gas sensing properties, J. Alloys Compd. 850 (2021) 156663, https://doi.org/10.1016/j.jallcom.2020.156663.

[42] Xiaolong Zhang, Yongbing Tang, Fan Zhang, Chun-Sing Lee, A novel aluminum–graphite dual-ion battery, Adv. Energy Mater. 6 (11) (2016) 1502588, https://doi.org/10.1002/aenm.201502588.

[43] Meng Wang, Chunlei Jiang, Songquan Zhang, Xiaohe Song, Yongbing Tang, Hui-Ming Cheng, Reversible calcium alloying enables a practical room-temperature rechargeable calcium-ion battery with a high discharge voltage, Nat. Chem. 10 (2018) 667–672, https://doi.org/10.1038/s41557-018-0045-4.

[44] Bangze Zhou, Zhanxu Liu, Chenchen Li, Mengsi Liu, Jiang Liang, Yanfen Zhou, Feng-Lei Zhou, Shaojuan Chen, Stephen Jerrams, Jianyong Yu, A Highly Stretchable and Sensitive Strain Sensor Based on Dopamine Modified Electrospun SEBS Fibers and MWCNTs with Carboxylation 7, 2021, p. 2100233, https://doi.org/10.1002/aelm.202100233.

[45] Yanfen Zhouab, Zhenhua Suna, Jiang Liang, Shaojuan Chena, Jianwei Ma, Fenglei Zhou, Flexible and conductive meta-aramid fiber paper with high thermal and chemical stability for electromagnetic interference shielding, Appl. Surf. Sci. 533 (2020) 147431, https://doi.org/10.1016/j.apsusc.2020.147431.

[46] Hao Cheng, Tianhao Li, Xuenuan Li, Jun Feng, Tingfang Tang, Danfeng Qin, Facile synthesis of Co_9S_8 nanocages as an electrochemical sensor for luteolin detection, J. Electrochem. Soc. 168 (2021), 087504, https://doi.org/10.1149/1945-7111/ac1813.

[47] Chao Xue, Juan You, Huimin Zhang, Shanbai Xiong, Tao Yin, Qilin Huang, Capacity of myofibrillar protein to adsorb characteristic fishy-odor compounds: effects of concentration, temperature, ionic strength, pH and yeast glucan addition, Food Chem. 363 (2021) 130304, https://doi.org/10.1016/j.foodchem.2021.130304.

[48] Li-Bin Hu, Xin-Yu Huang, Shan Zhang, Xue Chen, Xian-Hui Dong, He Jin, Zhen-Yu Jiang, Xiao-Ran Gong, Yi-Xuan Xie, Chen Li, Zong-Tao Chi, Wan-Feng Xie, MoO_3 structures transition from nanoflowers to nanorods and their sensing performances, J. Mater. Sci. Mater. Electron. 32 (2021) 23728–23736, https://doi.org/10.1007/s10854-021-06464-7.

[49] Yihan Yang, Jinchuan Liu, Xiaohong Zhou, A CRISPR-based and post-amplification coupled SARS-CoV-2 detection with a portable evanescent wave biosensor, Biosens. Bioelectron. 190 (2021) 113418, https://doi.org/10.1016/j.bios.2021.113418.

[50] Tingting Zhang, Zhijie Wang, Huijing Xiang, Xue Xu, Jing Zou, Chichong Lu, Biocompatible superparamagnetic europium-doped iron oxide nanoparticle clusters as multifunctional Nanoprobes for multimodal in vivo imaging, ACS Appl. Mater. Interfaces 13 (29) (2021) 33850–33861, https://doi.org/10.1021/acsami.1c07739.

[51] Zhuofu Deng, Binbin Wang, Yanlu Xu, Tengteng Xu, Chenxu Liu, Zhiliang Zhu, Multi-scale convolutional neural network with time-cognition for multi-step short-term load forecasting, IEEE Access 7 (2021) 88058–88071, https://doi.org/10.1109/ACCESS.2019.2926137.

[52] Zhuofu Deng, Chenxu Liu, Zhiliang Zhu, Inter-hours rolling scheduling of behind-the-meter storage operating systems using electricity price forecasting based on deep convolutional neural network, Int. J. Electr. Power Energy Syst. 125 (2021) 106499, https://doi.org/10.1016/j.ijepes.2020.106499.

[53] Xiansheng Zhang, Shehua Tong, Ming Chen, Recent advances of Zr based metal organic frameworks photocatalysis: energy production and environmental remediation, Coord. Chem. Rev. 448 (2021) 214177.

[54] G. Nicholas, Pavlopoulos, shining light on the role of shape-controlled nanomaterials in photocatalysis, Curr. Opin. Electrochem. 26 (2021) 100676.

[55] Min Yang, Fang Lu, Vinod Kumar Gupta, Biosynthesis of nano bimetallic Ag/Pt alloy from *Crocus sativus* L. extract: biological efficacy and catalytic activity, J. Photochem. Photobiol. B Biol. 212 (2020) 112025.

[56] Özgecan Erdem, Yeşeren Saylan, Adil Denizli, Molecularly imprinted nanoparticles based plasmonic sensors for real-time enterococcus faecalis detection, Biosens. Bioelectron. 126 (2019) 608–614.